Tamap Journal of Physical Science
http://www.tamap.org/

TJOPS-1811-01
Volume 2018, Article ID 2
Research Article

Long-Term X-Ray Variable Source J141648.7+522558 at Groth-Westphal Field

Nergis CESUR[1,*]

[1] *Department of Astrophysics / IMAPP, Radboud University Nijmegen, P.O.Box 9010, 6500 GL, Nijmegen, NL*

Received: 01.11.2018 • **Accepted**: 30.11.2018 • **Published Online:** 06.12.2018

Abstract: We analyzed X-ray archival data of J141648.7+522558 from Groth-Westphal Field, observed with X-ray telescopes of XMM-Newton and Chandra at nine different observations, with an emphasis on investigating the long-term flux and spectral variability of the source. We selected a southern nearby source with a 30-arcsec separation, J141649.4+522531, in an attempt to compare the fluxes and determination of any detector deficiency through its consistency. Both X-ray sources seem to have bright elliptical counterparts coinciding at their X-ray peak. By comparing the fluxes, the southern source J141649.4+522531 is observed to have a steady emission and a consistent flux value of about $F_X = 10.04\pm0.99\times10^{-14}$ erg cm^{-2} s^{-1} and a luminosity value of about $L_X=27.37\pm1.30\times10^{44}$ erg s^{-1} (at z=2.35) at nine epochs during 2000-2014. On the other hand, J141648.7+522558 has an emission of a flux value of about $F_X = 3.61\pm0.53\times10^{-14}$ erg cm^{-2} s^{-1} in the year 2000, but very faint in 2002, 2005 and 2014 observations by Chandra. The nature of this flux variability and the underlying physics is discussed by considering possible mechanisms to affect the emission dramatically.

Keywords: High energy astrophysics: galaxies: active, X-rays: galaxies

1. INTRODUCTION

The Extended Growth Strip region ($\alpha = 14^h\ 17^m$, $\delta = 52°\ 30'$) which is broadens "Groth-Wesphal Strip" to a size of $2° \times 15'$, has plenty of observations in X-rays and also multi-wavelength studies, thus, provides information to investigate nature of point sources. X-ray observations can provide useful information to understand the emission process and the physical conditions in the central engine of Active Galactic Nuclei (AGN). X-ray emission of an AGN is variable both in flux and in the spectral properties on very short time scales to years, and this variability is one of the defining characteristics of emitting region. Due to the spectral characteristic of each process is unique, long-term flux and spectral analysis is primary study to investigate the nature of an X-ray source and high spatial resolution X-ray telescopes such as *XMM-Newton* and *Chandra* provide opportunities to all these purposes. Multi-wavelength surveys are important for understanding the behavior of AGN because of their different wavelength emission mechanisms. With the help of these surveys, we found that our sources were identified as an infra-red sources in the study of Ashby et.al (2013).

The area of the northern source we chose for X-ray analysis as a detected X-ray source, J141648.7+522558 (with *IRAC ID* 056633), has two sources declared that one of them is *starbust-dominated AGN* (with *IRAC ID* 056633-1) and the other one is *normal galaxy hosting* AGN (with *IRAC ID* 056633-2) and the southern source J141649.4+522531 is a *Type-I AGN* (with *IRAC ID* 054089), in the multi-wavelength study of Almeida et.al (2009). On the other hand, they were identified as X-ray sources in the *Chandra GWS X-ray Catalogue* study of Nandra et. al (2005) in the source catalogue numbers with c6 and c7, respectively, where the northern source we chose in X-ray analysis, is detectable as a single region like in this study. J141648.7+522558 is referred to as northern source and J141649.4+522531 is referred to as southern source hereafter.

* Correspondence: N.Cesur@astro.ru.nl

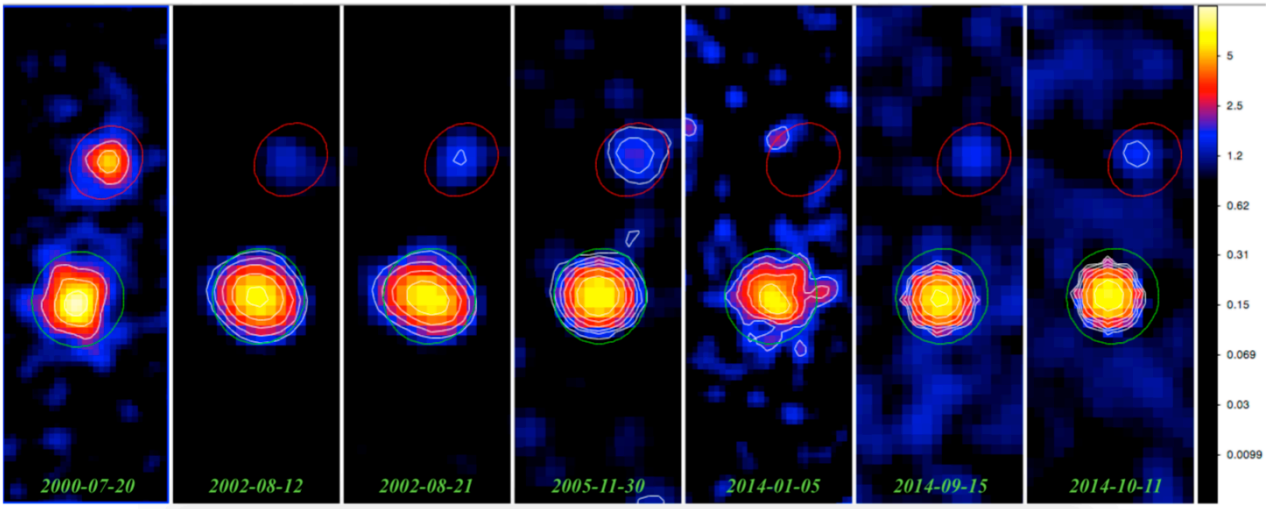

Figure 1: X-ray images of the two sources with contours, in chronological order. First image is combined image of event files of Obs.Id. 0127920401, 0127921001 and 0127921201 at the first epoch. The color scale corresponds the image counts. The background level subtracted lowest contour level is 3 times the image rms, and each higher contour is 1.75 times the previous contour level.

2. OBSERVATIONS AND DATA ANALYSIS

For our analysis, we used both archival Groth-Wesphal Strip Field *XMM-Newton* observations obtained from *XMM-Newton* Science Archive and *Chandra* observations obtained from *Chandra* Data Archive. Analyzing over different observations provide us a unique opportunity to calculate long-term flux and spectral variability. With different nine observations with relatively long exposure times compared the others, from *XMM-Newton* and *Chandra*, we have a significant time span about fourteen years. Summary of data set for *XMM-Newton* and *Chandra* is shown in Table 1.

Table 1: XMM-Newton and Chandra Log of Archival Groth-Westphal Strip Observation used in our study, chronologically.

Observatory	Obs. Id.	Obs. dates	Pointing direction RA/DEC (J2000)	Instrument	Exp. (sec)
XMM-Newton	0127920401	2000-07-20	14 17 12.01 +52 24 00.00	EPIC MOS	49981
XMM-Newton	0127921001	2000-07-21	14 17 12.01 +52 24 00.00	EPIC MOS	65711
XMM-Newton	0127921201	2000-07-23	14 17 12.01 +52 24 00.00	EPIC MOS	19588
Chandra	4357	2002-08-12	14 17 43.60 +52 28 41.20	ACIS-I	85440
Chandra	4365	2002-08-21	14 17 43.60 +52 28 41.20	ACIS-I	84830
Chandra	7236	2005-11-30	14 16 24.50 +52 20 02.59	ACIS-I	20640
XMM-Newton	0723860101	2014-01-05	14 17 11.04 +52 25 41.80	EPIC MOS	30300
Chandra	16027	2014-09-15	14 17 11.00 +52 25 41.90	ACIS-S	26960
Chandra	17487	2014-10-11	14 17 11.00 +52 25 41.90	ACIS-S	33070

XMM-Newton data analysis was performed by using *XMM-Newton* Scientific Analysis System (XMMSAS) v14.0.0 provided by the *XMM-Newton* Science Operations Center (SOC) and *Chandra* analysis was performed by using CIAO 4.8 and CALDB 4.7.0 provided by the *Chandra* X-Ray Center (CXC), imaging application SAOImage DS9 v7.3.2 and spectral analysis software XSPEC v12.8.2. *XMM-Newton* event list files for EPIC MOS cameras are created by using *emchain* task. We selected only good event patterns for imaging ≤ 12 for EPIC MOS. As in the standard procedure by *Chandra X-Ray Center*, we reprocessed our events list *Chandra* files by using the script *Chandra*-repro and for restricting the energy ranges and creating the images *dmcopy* script were used on the event files, respectively.

We merged the *XMM-Newton* event files of Obs.Id. 0127920401, 0127921001 and 0127921201 to increase detectability and corrected position offsets. Since the chip gap blocks majority of the northern source and partly the southern source, we did not use EPIC PN data in *XMM-Newton* analysis.

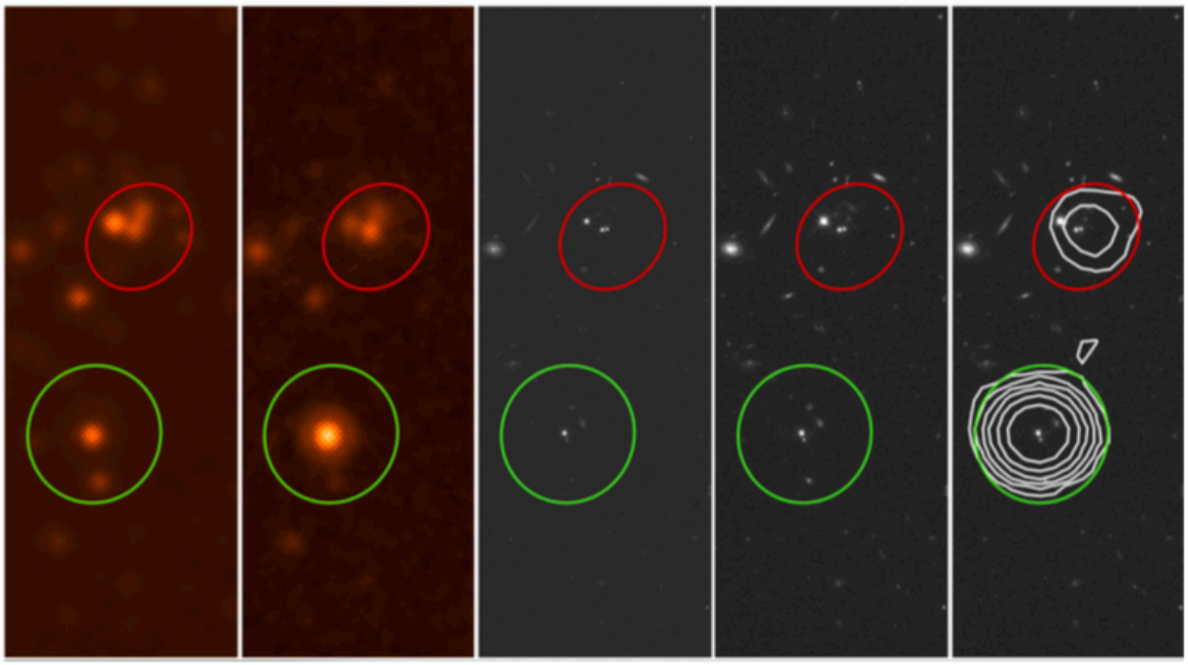

Figure 2: 3.6 μm and 8.0 μm mosaic images by SST/IRAC in 2003 December and 2004 June-July, V and I Band images by Hubble Space Telescope (here after HST)/ACS mosaics of the Extended Groth Strip between 2004 June and 2005 March, respectively. The image on the far right shows plotted November 2005 X-ray contours on I Band image by HST/ACS.

2.1 Imaging Analysis

Morphological comparisons between the X-ray emission images may provide convenience to investigate the nature of the X-ray emission, which divides each of our X-ray sources into three main components. For our analysis, a bright core source that extracts highest count rate *(yellow)*, soft X-ray extended emission surrounding the core source *(orange/red)* and very weak diffuse emission in outer layer of the object that extracts lowest count rate *(dark blue)* are shown in Figure 1. Hence, we plotted contours on 3 arcsec Gaussian smoothed X-ray images through the observation dates for the purpose of emphasize the variability and fading, to show difference in emissions. As seen in the related figure, contours of the northern source are changing through the epochs. Furthermore, we put the X-ray contours of the 2005 November observation on Hubble Space Telescope (hereafter HST)/Advanced Camera for Surveys (ACS) image which obtained between 2004 June and 2005 March (see Figure 2) to bring out the fact that the northern source can be detectable in other wavelengths while it has very weak X-ray emission.

Isolating different components and fitting them individually, such as extracting the core emission and the emission surrounding the core, may provide best analysis because of removing complexity in spectral data as in the doctoral dissertation of Fan Yi (2007). But while we have complicated structure with small area to extract the core region and not enough count rates, it is in- appropriate to fit the spectrum with these small degrees of freedom and low statistical significance in line with this analysis method. So fitting the spectrum roughly, as region is a whole body with a power-law continuum, might be enough to a general approach.

Figure 2 shows 3.6 μm and 8.0 μm images were obtained in two epochs 2003 December and 2004 June-July by Spitzer Space Telescope (SST)/Infrared Array Camera (IRAC) and HST/ACS mosaics of the Extended Groth Strip, respectively. The figure shows that three source can be observable in the selected region of the northern source from left to right J141649.08+522559.7, J141648.75+522558.9 and J141648.66+522601.4, respectively. In X- ray detections, their images are overlapped so detecting sources as a single source is failed. The source region surrounding with J141648.75+522558.9 and J141648.66+522601.4 are confirmed as *normal galaxy hosting AGN* (with *IRAC ID* 056633 2) in the multi-wavelength study of Almeida et.al (2009), as mentioned before.

Figure 3 shows the central X-ray emissions of the sources in seven bands. These images clearly show the emission fading at X-ray energies higher than 5 keV, and up to 5 keV the core emission and surrounded extended X-ray emission is obviously seen. We used *XMM-Newton* merged images of observation id (Obs.Id.) 0127920401,

0127921001 and 0127921201 to generate these images with reduced noise by this way, which northern source is prominent in with its highest count rates comparing with other observations.

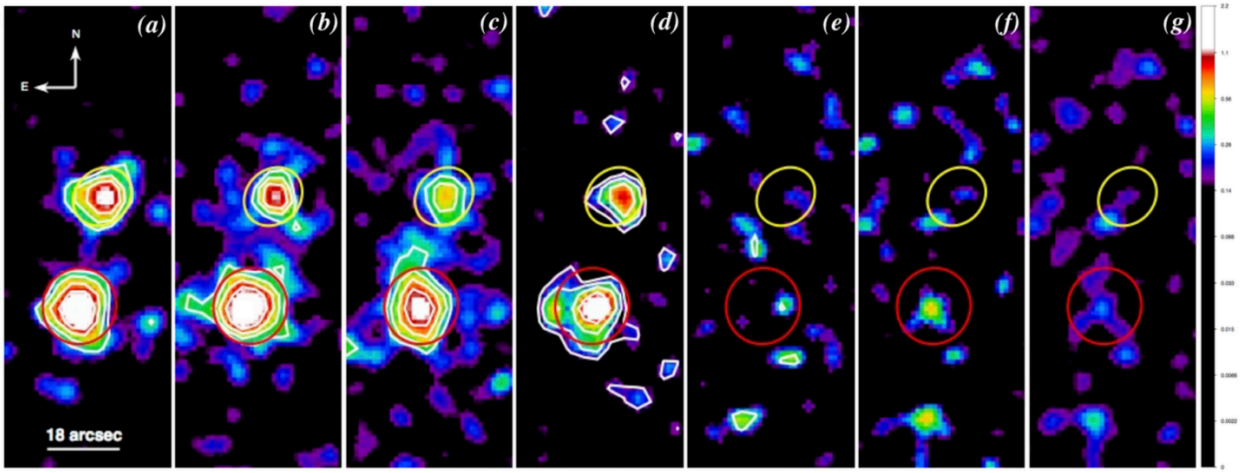

Figure 3: X-ray images of the both sources in various energy bands. The color scale corresponds the image counts. Contours are plotted on 4 arcsec Gaussian smoothed images. The background level subtracted lowest contour level is 3 times the image rms, and each higher contour is 1.50 times the previous one. The energy ranges used are (a) 0.5-1.0 keV, (b) 1.0-1.5 keV, (c) 1.5-2.0 keV, (d) 2.0-2.5 keV, (e) 6.0-6.5 keV, (f) 5.0-8.0 keV and (g) 5.0-10.0 keV.

2.2. Spectral Analysis and Calculation of the Flux

In order to investigate the flux differences of the northern source, we inspected by spectral analysis both sources with *XSPEC* and in accordance with this purpose, we created simple energy spectra for both *XMM- Newton* and *Chandra* observations data. The counts of the northern source is extracted from an area of 163.35 arcsec^2 and the counts of the southern source is extracted from an area of 274.67 arcsec^2 ellipse centered on their X-ray peaks. Because of the low count rates of the sources, a simple source-free ring of 156.09 arcsec^2 regions, properly near the both sources, represented background emission. Owing to low count rates are effective on determining the best results, extracted spectra were grouped according to providing the best chance of probability, best-fit spectra and fair model parameters.

For *XMM-Newton* observations, we created spectrum and background files of sources with *evselect* task, Ancillary Response Files (ARFs) with *arfgen* task and Response Matrix Files (RMFs) with *rmfgen* task in *SAS*. For each *Chandra* observations, we generated ARFs and RMFs for both source and background with *specextract* script in in *CIAO*. Due to each sources nearly have a consistency with their spectral parameters in all Chandra observations after 2000, *XMM-Newton* observations, we also merged spectrum files of these observations for the purpose of presenting the characterization of spectra clearly. Without this approach, the northern source is so dim in *Chandra* observations after July 2000, *XMM-Newton* observations, it is hard to fit the model to spectrum with small degrees of freedom and so, well fitted spectra of sources can be shown properly with this process. Hence, we use *combine spectra* task in *CIAO* to combine spectrum files which are source spectra, associated source ARFs and RMFs; background spectra, associated background ARFs and RMFs. After creating all spectral files of each observation, we define the channel grouping with the task *grppha* within the *FTOOLS*. Still having poor counts per channel, we used Cash statistics in our analysis (Cash 1979). Since X-ray emission from AGNs is a non-thermal emission, to roughly characterize the spectral shapes, we chose a standard approach for spectral fitting of sources with absorbed *POWERLAW* model in *XSPEC* (Arnaud 1996). The *WABS* model was used for modeling the Galactic absorption (fixed at N_H=1.04×10^{20} cm^{-2}). In *XMM-Newton* data spectral analysis, we allowed to be free the normalizations among different cameras. Figure 4 shows the spectral fittings for each epoch.

Finally, the fluxes were obtained from the count rate assuming the absorbed *POWERLAW* model and we used the four basic energy bands given in *Chandra GWS X- Ray Catalogue* (Nandra et.al 2005) to get comparable fluxes with the catalogue through the observation dates, based on 1σ error. All fluxes and photon indexes of both sources are given in Table 2, respectively.

Figure 4: Source spectrum and residuals. The red-black, and single black spectrum are from *XMM- Newton* and *Chandra,* respectively.

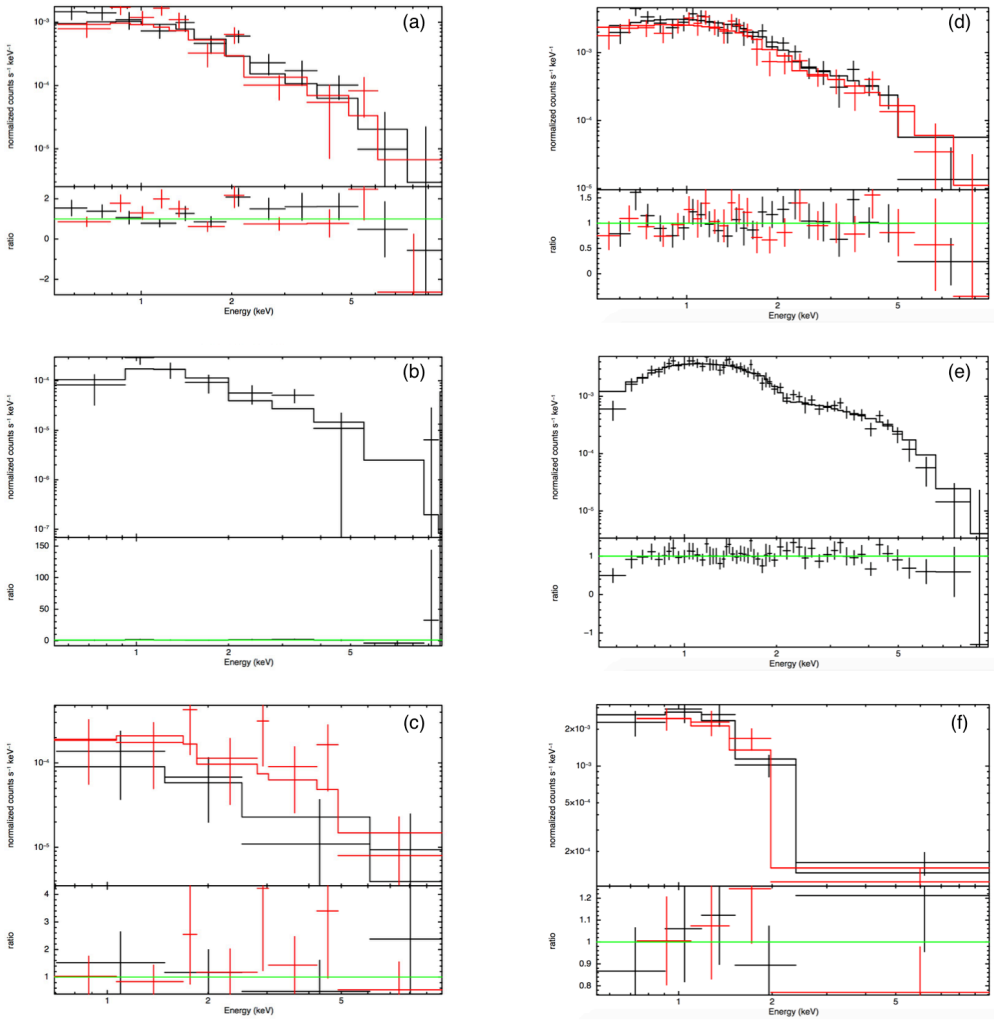

Table 2: Flux and Photon Index for northern source J141648.7+522558 and southern source J141649.4+522531, respectively. (1) 0.5-10.0 keV flux full band; (2) 0.5-2.0 keV flux soft band; (3) 2.0-10.0 keV flux hard band; (4) 5.0-10.0 keV flux ultra hard band. All fluxes are in 10^{-14} ergs cm^{-2} s^{-1} units. (5) Photon index of the power-law distribution. The errors represent the 1 σ confidence interval.

RA (J2000)	DEC (J2000)	Observatory	Obs. Date	Epoch No.	$F_{0.5\text{-}10}$ (1)	$F_{0.5\text{-}2}$ (2)	$F_{2\text{-}10}$ (3)	$F_{5\text{-}10}$ (4)	$\Gamma_{0.5\text{-}10}$ (5)	c-stat/dof
J141648.7	+522558									
		XMM-Newton	2000-07-20/21/23	1	$4.34^{+0.52}_{-0.30}$	$1.79^{+0.19}_{-0.13}$	$2.55^{+0.50}_{-0.38}$	$1.16^{+0.30}_{-0.20}$	$1.89^{+0.22}_{-0.21}$	120.40/110
		Chandra	2002-08-12	2	<0.5	<0.5	<0.5	<0.5	$3.23^{+3.59}_{-1.63}$	6.93/6
		Chandra	2002-08-21	3	$0.71^{+0.20}_{-0.12}$	<0.5	<0.5	<0.5	$2.04^{+0.68}_{-0.59}$	13.72/21
		Chandra	2005-11-30	4	$0.83^{+1.07}_{-0.36}$	<0.5	$0.57^{+0.94}_{-0.37}$	<0.5	$1.62^{+2.63}_{-1.10}$	5.67/7
		XMM-Newton	2014-01-05	5	$3.16^{+1.35}_{-1.36}$	<0.5	$2.76^{+1.88}_{-1.35}$	$1.80^{+1.08}_{-0.92}$	$0.85^{+0.85}_{-0.70}$	10.12/15
		Chandra	2014-09-15	6	$0.84^{+0.32}_{-0.53}$	<0.5	$0.76^{+0.59}_{-0.59}$	$0.52^{+0.27}_{-0.51}$	$0.67^{+8.37}_{-1.37}$	1.44/4
		Chandra	2014-10-11	7	<0.5	<0.5	<0.5	<0.5	$2.24^{+2.27}_{-1.90}$	11.57/10
J141649.4	+522531									
		XMM-Newton	2000-07-20/21/23	1	$11.02^{+0.90}_{-0.73}$	$3.77^{+0.18}_{-0.19}$	$7.24^{+0.76}_{-0.66}$	$3.57^{+0.33}_{-0.42}$	$1.68^{+0.12}_{-0.11}$	61.55/83
		Chandra	2002-08-12	2	$9.26^{+0.74}_{-0.83}$	$3.12^{+0.25}_{-0.24}$	$6.13^{+0.42}_{-0.70}$	$3.05^{+0.56}_{-0.48}$	$1.67^{+0.17}_{-0.17}$	18.89/21
		Chandra	2002-08-21	3	$8.77^{+0.68}_{-0.57}$	$3.08^{+0.23}_{-0.25}$	$5.69^{+0.87}_{-0.68}$	$2.78^{+0.69}_{-0.30}$	$1.71^{+0.19}_{-0.18}$	5.55/8
		Chandra	2005-11-30	4	$12.09^{+1.99}_{-1.69}$	$3.94^{+0.55}_{-0.45}$	$8.15^{+2.35}_{-1.18}$	$4.10^{+1.36}_{-1.02}$	$1.63^{+0.37}_{-0.33}$	2.04/2
		XMM-Newton	2014-01-05	5	$9.66^{+1.43}_{-0.83}$	$3.58^{+0.30}_{-0.33}$	$6.08^{+1.41}_{-1.03}$	$2.90^{+0.95}_{-0.60}$	$1.77^{+0.25}_{-0.22}$	4.56/6
		Chandra	2014-09-15	6	$10.07^{+1.33}_{-0.88}$	$3.60^{+0.29}_{-0.28}$	$6.48^{+1.40}_{-1.27}$	$3.14^{+0.71}_{-0.67}$	$1.73^{+0.27}_{-0.25}$	4.56/6
		Chandra	2014-10-11	7	$11.63^{+1.09}_{-1.11}$	$3.78^{+0.30}_{-0.28}$	$7.85^{+1.20}_{-1.27}$	$3.95^{+0.83}_{-0.68}$	$1.63^{+0.18}_{-0.18}$	14.70/20

3. RESULTS

The four *XMM-Newton* and five *Chandra* observations were analyzed in this work spanned a period of fourteen years from 2000 to 2014. The northern source varied in flux by 3.61×10^{-14} *ergs cm*$^{-2}$ *s*$^{-1}$ to 0.19×10^{-14} *ergs cm*$^{-2}$ *s*$^{-1}$ and the southern source has a mean flux value about $10.04 \pm 0.99 \times 10^{-14}$ *ergs cm*$^{-2}$ *s*$^{-1}$. We examined the light

curves extracted from selected source area for both *XMM-Newton* and *Chandra* data within the energy range of 0.5-10.0 keV and found no significant flares. According to Figure 3, for the energy ranges 6.0- 6.5 keV, 5.0-8.0 keV and 5.0-10.0 keV, both sources are too faint to detect in these X-ray bands, but their count rates are still higher than the background level count rates. The fluxes of the northern source are nearly under steady state after first epoch. In case, the southern source has a consistency through all epochs except the fourth and fifth epochs where there is an increase in flux rate that may be caused by possible contamination by signal to noise ratio emission.

All observed spectrum of the north and south sources are shown in Figure 4 with all *Chandra* merged spectra for the purpose of presenting the characterization of the spectra clearly, as referred before in Section 2.2. Inspections of the spectral shapes over the fourteen years of *XMM-Newton* and *Chandra* data revealed that the spectra of sources did not change significantly as seen in the Figure 4, except 2014 *XMM- Newton* observation which is very different from the others and shows that the model did not give an acceptable fit for the northern source. Besides, spectrum of the southern source indicates that there was an abrupt change in the slope for emission above 2 keV, which showed a much harder emission in other observations. For X-ray spectra of both sources, any thermal model did not satisfy a thermal component with high and invalid error rates and unrealistically high values of temperature.

4. CONCLUSION

In this paper we present X-ray flux and spectral analysis of J141648.7+522558 and J141649.4+522531 with the intent of investigating the confirmed flux and morphological variability of J141648.7+522558. The X-ray continuum of the both sources appears to have a non-thermal, power-law form. The northern source we chose for X-ray analysis, which refers starburst dominated AGN and a normal galaxy hosting AGN according to the multi-wavelength study of Almeida et.al (2009), is going under a consistent fading through epochs after the year 2000, XMM-Newton observations. In the view of such information with this complex structure, it is not clear to understand which mechanism drives the X-ray emission and variability behavior in this region. On the other hand, the results, X-ray flux variability and fading through epochs, are consistent with the study of Almeida et.al (2009) that suggested flux contamination with extra emission coming from the companion and obscured starburst-dominated AGN situations. X-ray telescopes for future missions with longer exposures and higher photon counts are required for a clear-cut conclusion with better statistics to understand the intrinsic nature of this long-term flux variability.

Acknowledgements: NC would like to thank YTU Scientific Research and Project Office (BAP) funding with contract numbers FYL-2018-3309 for financial support. Also, NC thanks the anonymous referee for useful suggestions on the manuscript.

REFERENCES

[1] Ashby M. L. N. et al., 2013, ApJS, 209, 22
[2] Almeida C., Pérez García A. M., Acosta-Pulido J. A. 2009, AJ, 137, 179
[3] Nandra K., Laird E.S., Adelberger K., et. al, Mon. Not. R. Astron. Soc., 356, 568-586 (2005)
[4] Fan, Yi; Thesis (Ph.D.), Technische Universitat Munchen, 2007, Advisor: Hasinger, Gunther
[5] Arnaud K. A., 1996, in Astronomical Society of the Pacific Conference Series, Vol. 101, Astronomical Data Analysis Software and Systems V, Jacoby G. H., Barnes J., eds., p. 17
[6] Cash,W. 1979, ApJ, 228, 939